communications earth & environment

A Nature Portfolio journal

Article

https://doi.org/10.1038/s43247-026-03507-x

Warmer Atlantic Water intrusion energizes the Arctic Eurasian Basin

Jiao Chen [1,2,7], Xuezhu Wang [3,4,7], Qiang Wang [2] ✉, Xinyue Li[5], Vasco Müller [2], Sergey Danilov [2], Xidong Wang [1] & Thomas Jung [2,6]

Climate warming is expected to weaken ocean circulation by suppressing deep-ocean eddy activity at mid and low latitudes. However, the future evolution of deep-ocean dynamics in the rapidly changing Arctic remains unclear. Here, we use 1-km-resolution simulations to show that the deep Arctic Ocean is projected to become substantially more energetic, particularly in the Eurasian Basin, in stark contrast to global mean trends. This increase in kinetic energy is driven primarily by intensified mesoscale eddy activity, fueled by enhanced lateral density gradients and available potential energy resulting from progressing Arctic Atlantification. Deep-ocean eddies account for more than half of the projected rise in Arctic total kinetic energy. The projected enhancement of eddy activity in both upper and deep layers implies that Arctic Atlantification could influence the Arctic Ocean and sea ice through dynamic pathways beyond simply supplying oceanic heat to the Arctic Ocean.

Mesoscale ocean eddies are fundamental components of the climate system, mediating interactions across a wide range of spatial and temporal scales[1]. These energetic vortices, which typically span 10–100 km in diameter and last weeks to months, contain the majority of the kinetic energy of the ocean and are ubiquitous features of global circulation[2,3]. By redistributing heat, salt, and tracers both vertically and laterally, eddies influence water mass transformation, regulate stratification, and shape large-scale ocean circulation patterns[4–7]. They contribute to the ventilation of the thermocline, modulate the uptake and storage of heat and anthropogenic carbon, and enhance upper-ocean productivity[8–10].

Satellite observations have revealed that surface mesoscale eddy activity in eddy-rich regions of the global ocean has increased over the past three decades[11]. Climate model projections indicate that this trend will continue in most of these regions under future warming scenarios[12]. In contrast to the upper ocean, eddy activity in the deep ocean is projected to decline due to reductions in available potential energy associated with enhanced vertical stratification[13]. Despite the intensification of the upper ocean circulation[12,14], the increasingly quiescent deep ocean results in a substantial reduction in the global ocean's total kinetic energy (TKE)[13]. This underscores the critical role of mesoscale eddies in modulating the anthropogenic changes in the ocean's kinetic energy budget.

The Arctic is experiencing the most rapid climate change on Earth[15,16]. In the Arctic, ocean eddies play an important role in modulating sea ice basal melting, the ocean's physical environment, and marine ecosystems[17,18]. Although observations remain limited, mesoscale eddies are recognized as a persistent feature of the Arctic Ocean[19–23]. Observational and modeling studies reveal widespread eddy activity in the Arctic Ocean, with notable spatial and temporal variability[24–27]. Sea ice cover suppresses eddy growth and promotes the dissipation of existing eddies at the surface, weakening surface eddy activity beneath the ice[28,29]. Under future warming scenarios, however, eddy kinetic energy (EKE) in the upper Arctic Ocean is projected to increase markedly due to sea ice retreat and enhanced baroclinic instability[30].

In the early 21st century, the Arctic Ocean underwent substantial changes in its Atlantic Water layer, a process referred to as Arctic Atlantification[31–33]. This phenomenon is characterized by the warming of the Atlantic Water layer and an upward shoaling of its upper boundary[33,34]. Arctic Atlantification is projected to intensify under continued climate warming[16], further contributing to the decline of Arctic sea ice[35]. However, how the progression of Atlantification influences the Arctic Ocean kinetic energy budget, especially eddy dynamics, under future climate change remains largely unknown and represents a critical uncertainty in projections of Arctic changes. In particular, it is unclear whether the deep Arctic Ocean will become more quiescent, as is expected in lower-latitude oceans in the future[13], or follow an opposite trend. This knowledge gap stems from the limited ability of current high-resolution climate models to resolve mesoscale eddies in the Arctic Ocean, where the baroclinic Rossby radius is exceptionally small[36,37]. Typical mesoscale eddies observed in the Arctic

[1]College of Oceanography, Hohai University, Nanjing, China. [2]Alfred Wegener Institute, Helmholtz Centre for Polar and Marine Research, Bremerhaven, Germany. [3]Donghai Laboratory, Zhoushan, China. [4]Laboratory of Polar Ecosystem and Climate Change, Ministry of Education, Shanghai Jiao Tong University, Shanghai, China. [5]Max Planck Institute for Meteorology, Hamburg, Germany. [6]Department of Physics and Electrical Engineering, University of Bremen, Bremen, Germany. [7]These authors contributed equally: Jiao Chen, Xuezhu Wang. ✉e-mail: qiang.wang@awi.de

Ocean have radii of less than 10 km[21], and modeling studies suggest that a horizontal resolution of approximately 1 km is needed to adequately resolve these features[26,38].

In this study, we use a global multi-resolution sea ice-ocean model, configured with 1 km eddy-rich resolution in the Arctic Ocean, to investigate the response of deep Arctic Ocean dynamics to future climate warming under the high-emission Shared Socioeconomic Pathway 5-8.5 (SSP5-8.5) scenario[39]. Our results show that EKE in the deep Eurasian Basin increases in a warming world, in contrast to the decline in deep-ocean eddy activity at lower latitudes. This intensification is primarily driven by enhanced baroclinic instability associated with Arctic Atlantification, which increases available potential energy and strengthens energy conversion processes.

Results

Increasing kinetic energy in the deep ocean

This study employs simulations with kilometer scale horizontal resolutions. First, a global model simulation with an eddy-permitting medium horizontal resolution of 4.5-km in the Arctic Ocean was conducted, spanning from the historical period to the end of the 21st century (see "Methods"). The future projection was based on the high-emission SSP5-8.5 scenario. Then eddy-resolving simulations with a finer 1 km horizontal resolution were initialized using transient results from the medium-resolution run, focusing on two specific time slices. These slices represent the present-day climate (2012–2015) and a future warming scenario (2092–2095), respectively. The 1 km resolution allows us to resolve mesoscale eddies across most of the Arctic Ocean, with the exception of shallow shelf seas[26]. This high-resolution setup enables a detailed examination of both the spatial distribution and temporal evolution of mesoscale activities under climate change.

To assess how the ocean dynamics will evolve in a changing climate, we examine the kinetic energy in two ocean layers: the upper layer (0–100 m) and the deep layer (100–1000 m). We focus our analysis on the upper 1000 m because we find that future kinetic energy changes are pronounced in this depth range as we show below. During the present-day period (2012–2015), the Atlantic Water layer in the Eurasian Basin resides between approximately 100 m and 1000 m depths[40], as indicated by the vertical locations of 0 °C temperature (Supplementary Fig. 1a). The upper boundary of the Atlantic Water layer has started to shoal since the last decade[34,41], and this tendency is projected to continue in the future[16]. By the late 21st century, the annual mean temperature in the upper ocean is projected to rise above 0 °C, and the warm Atlantic Water layer also extends beyond 1000 m depth (Supplementary Fig. 1). Therefore, the deep layer in our analysis approximates the present-day depth range of the Atlantic Water layer in the Eurasian Basin.

Under the future warming scenario, the model projects an increase in TKE in the deep layer of the Arctic Ocean, attributed to increases in both mean kinetic energy (MKE) and EKE (Fig. 1). The increase in kinetic energy is widespread across the Arctic, but its magnitude exhibits pronounced spatial heterogeneity. Intensification of both mean circulation and eddy activity is particularly evident along major ocean currents that follow bottom bathymetric features, including the Atlantic Water Boundary Current (AWBC) along the Eurasian continental slope, the Atlantic Water return current along the Lomonosov Ridge, and the shelfbreak current in the western Arctic. Compared to MKE, EKE contributes more substantially to the projected TKE increase in most regions of the Arctic (Fig. 1e, f). The strongest enhancement of EKE is projected in the Eurasian Basin (Fig.1c, f). As found in previous studies[30], eddy activity and mean circulation in the upper layer of the Arctic Ocean are also projected to intensify (Supplementary Fig. 2).

Globally, the mean EKE in the deep ocean is projected to decline[13], although an increase is expected near the surface[12]. In contrast, our high-resolution simulations project an increase in EKE over both upper and deep layers of the Arctic Ocean (Fig. 1 and Supplementary Fig. 2), highlighting the Arctic as a regional exception compared to most mid- and low-latitude eddy-rich regions.

The projected increases in TKE, MKE and EKE over a large depth range under the future warming scenario are more clearly illustrated in the time-depth plots of kinetic energy shown in Fig. 2a–c. In the eddy-permitting simulation with a horizontal resolution of 4.5-km, TKE in the Eurasian Basin exhibits a long-term increasing trend throughout the 21st century, primarily attributed to an increase in EKE. At eddy-resolving resolution of 1 km, the projected intensification in TKE by the end of the

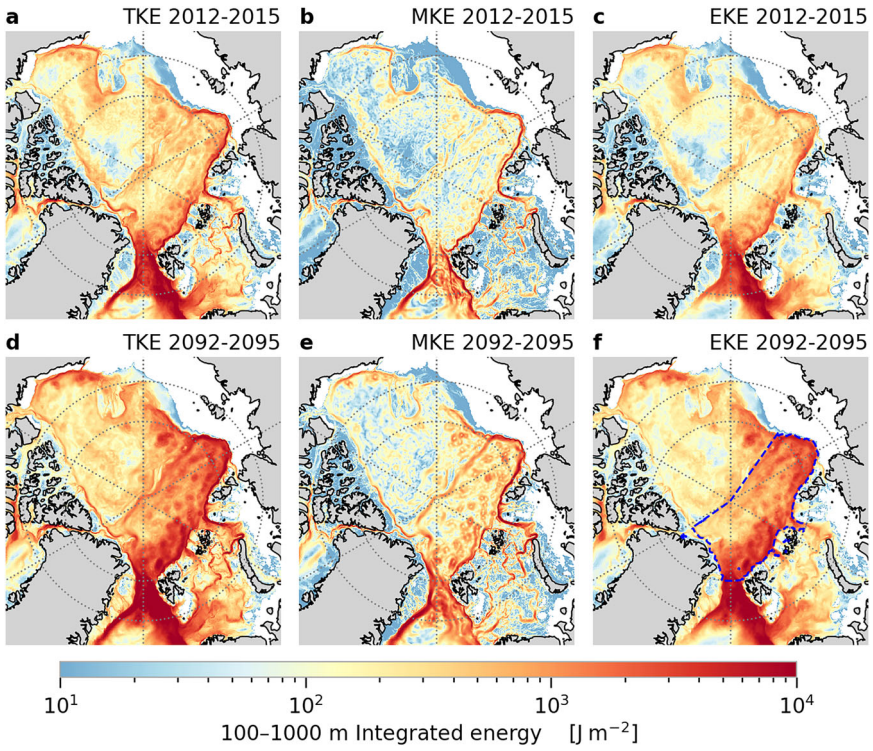

Fig. 1 | Intensification of deep Arctic Ocean kinetic energy in a warming world. Spatial pattern of vertically integrated (**a**) total kinetic energy (TKE), (**b**) mean kinetic energy (MKE) and (**c**) eddy kinetic energy (EKE) in the deep Arctic Ocean (100–1000 m) averaged over the time period of 2012–2015. **d**–**f** Same as (**a**–**c**), but for the time period of 2092–2095. The blue dashed line in (**f**) depicts the Eurasian Basin region used for mechanistic understanding.

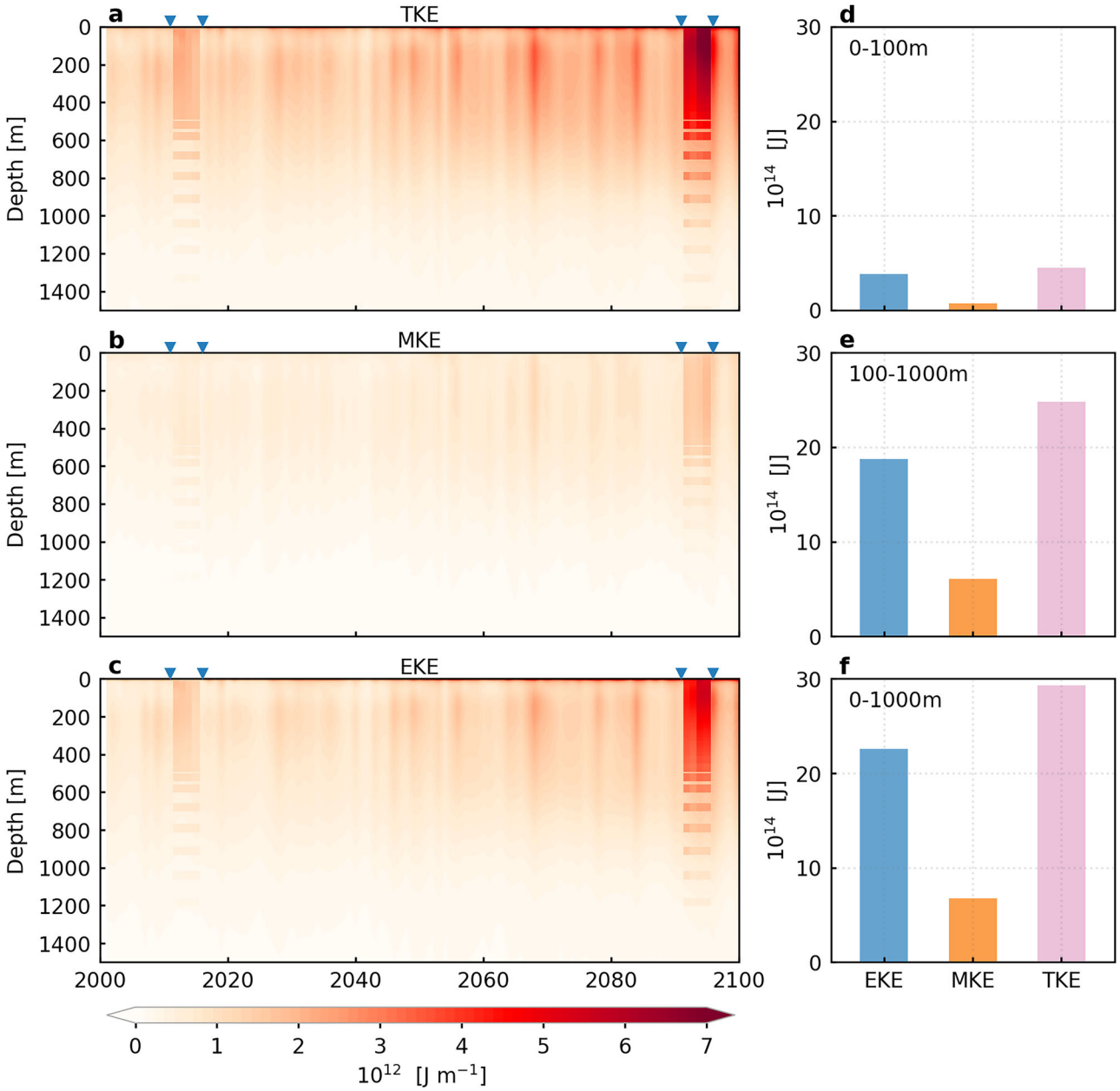

Fig. 2 | Increase in kinetic energy across the Eurasian Basin water column dominated by enhanced eddy kinetic energy (EKE). Time-depth plots of horizontally integrated (**a**) total kinetic energy (TKE), (**b**) mean kinetic energy (MKE) and (**c**) EKE over the Eurasian Basin. The background displays results from the 4.5-km resolution simulation, while the 1-km resolution simulation results are overlaid as small squares for the two time slices of 2012–2015 and 2092–2095. Blue triangles indicate the start and end points of each time slice. Future changes in horizontally and vertically integrated kinetic energy between 2012–2015 and 2092–2095 in (**d**) the upper layer (0–100 m), (**e**) the deep layer (100–1000 m) and (**f**) entire upper 1000 m depth.

century is substantially greater, mainly due to a stronger enhancement of EKE. This highlights the importance of resolving mesoscale processes in accurately capturing the Arctic Ocean's kinetic energy response to climate warming. While the increase in EKE diminishes with depth, it remains substantial in the upper 1000 m and is still discernible below (Fig. 2a–c).

In both the upper layer and the deep layer of the Eurasian Basin, the projected increase in TKE is primarily due to the increase in EKE (Fig. 2d–f). In the deep layer of the Eurasian Basin, approximately 75% of the TKE increase between the periods 2012–2015 and 2092–2095 can be attributed to enhanced EKE. This dominant contribution of EKE indicates that the projected TKE increase is primarily driven by intensified mesoscale dynamics, rather than by a strengthening of the mean flow. A similar relative contribution of EKE to TKE is found when considering the whole Arctic Basin, defined as the basin area with bottom bathymetry deeper than 200 m (Supplementary Fig. 3). The TKE in the whole Arctic Basin is projected to increase by approximately 140%. Of this total increase, around 80% is attributable to enhanced EKE, with about 60% specifically resulting from increased EKE in the deep layer. The most notable increase in deep-layer EKE is found in the Eurasian and Makarov Basins (Fig. 1c, f).

Enhanced baroclinic instability associated with Atlantic Water

Mesoscale eddies are primarily generated by baroclinic and barotropic instabilities[42,43]. Accordingly, EKE is sustained through two principal energy conversion pathways: from eddy available potential energy (EAPE) via baroclinic instability ($C_{\mathrm{EAPE}\rightarrow\mathrm{EKE}}$), and from MKE via barotropic instability ($C_{\mathrm{MKE}\rightarrow\mathrm{EKE}}$), as defined in Eqs. (4) and (5). We analyzed these energy conversion rates (Fig. 3) to identify the dominant mechanisms behind the markedly enhanced EKE found in the deep Arctic Ocean.

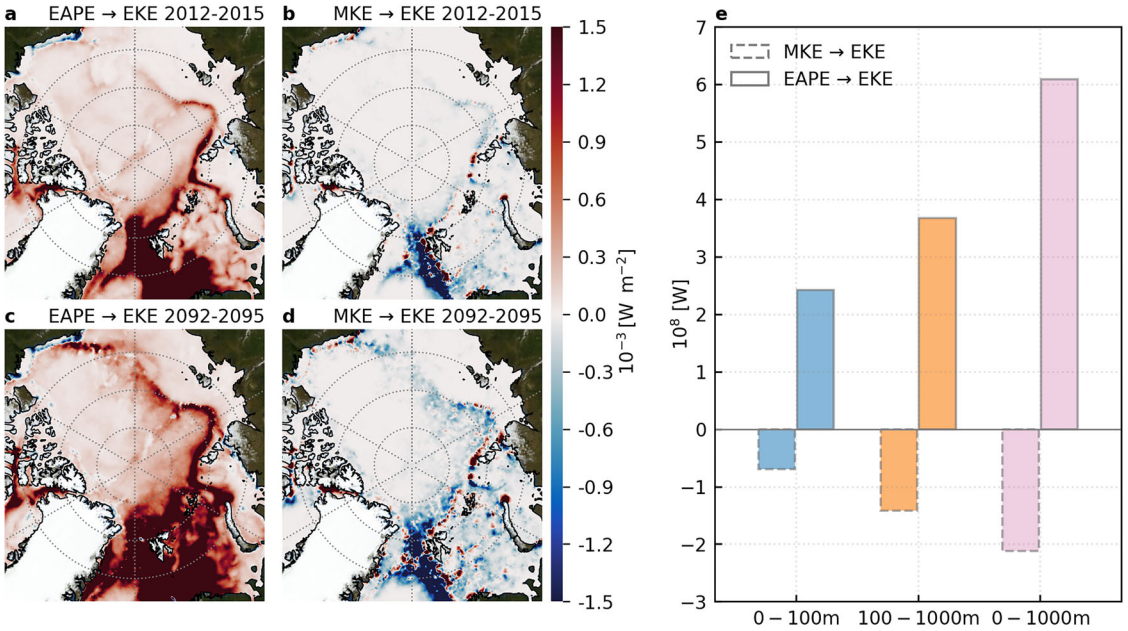

Fig. 3 | Enhanced mesoscale eddy activity mainly due to increased baroclinic instability. Spatial patterns of energy conversion rates (**a**) from eddy available potential energy (EAPE) to eddy kinetic energy (EKE) and (**b**) from mean kinetic energy (MKE) to EKE for the period 2012–2015. The vertical integration is over the 100–1000 m depth range. **c**, **d** Same as (**a**, **b**), but for the period 2092–2095. Negative values of the barotropic conversion indicate energy transfer from EKE to MKE. **e** Changes of energy conversion rates between the two time periods integrated over the Eurasian Basin.

The vertically integrated energy conversion rate from EAPE to EKE ($C_{EAPE\rightarrow EKE}$) is positive throughout the deep layer of the Arctic Ocean and exhibits a spatial pattern closely aligned with that of EKE, with enhanced values along bottom bathymetric slopes (Fig. 3a). This conversion rate is intensified across the basin under the future scenario, with the strongest amplification occurring in regions where historical values are already relatively high, particularly along the Eurasian continental slope (Fig. 3c). The energy conversion rate between MKE and EKE ($C_{MKE\rightarrow EKE}$) is also larger along bottom bathymetric slopes, but remains much weaker in magnitude than $C_{EAPE\rightarrow EKE}$ (Fig. 3a, b). Moreover, $C_{MKE\rightarrow EKE}$ exhibits both positive and negative values (Fig. 3b, d), indicating a spatially variable regime where eddies can either extract energy from or feed energy back into the mean flow. In particular, negative values of $C_{MKE\rightarrow EKE}$ indicate an inverse barotropic energy transfer, whereby kinetic energy is transferred from mesoscale eddies to the mean flow, contributing to the strengthening of the mean circulation. Such inverse energy transfer has also been observed in boundary currents and regions with strong topographic constraints in other parts of the global ocean[44,45]. This term is projected to intensify within the core of the AWBC along the Eurasian continental slope, while weakening over broader areas of the basin interior (Fig. 3b, d). Therefore, the future increase in $C_{EAPE\rightarrow EKE}$ is the primary driver of the projected enhancement in mesoscale activities in the deep Eurasian Basin.

To further elucidate the projected increase in EKE within the Eurasian Basin, we compared energy conversion rates between the periods 2012–2015 and 2092–2095. Under the future scenario, $C_{EAPE\rightarrow EKE}$ in the Eurasian Basin increases by approximately 61% (Fig. 3e and Supplementary Fig. 4). At the same time, the negative $C_{MKE\rightarrow EKE}$ is projected to increase in magnitude by nearly threefold. Despite this, the increase in $C_{EAPE\rightarrow EKE}$ dominates the energy budget (Fig. 3e), supporting the enhancement of eddy activity in the deep layer. These results highlight the leading role of intensified baroclinic instability, particularly associated with the Atlantic Water in the Eurasian Basin, in driving the projected increase in deep ocean EKE.

EKE in the upper layer also increases primarily due to enhanced baroclinic instability (Fig. 3e and Supplementary Fig. 4). Li et al. found that changes in upper-layer eddy activity are mainly driven by stronger eddy growth and reduced dissipation associated with sea-ice decline, and in the Amerasian Basin they are further enhanced by increased potential energy due to greater freshwater storage[30]. The maximum density stratification effectively separates the modes of baroclinic instability in the upper and deep layers, thereby confining the influence of surface friction to the surface layer[29,46]. In the Eurasian Basin, the maximum density stratification, located within the top 50 m, is projected to further increase (Supplementary Fig. 5), associated with enhanced salinity stratification (Supplementary Fig. 1), reinforcing the separation of instability modes between layers. This supports our focus on the deep layer as the primary domain for explaining future increases in eddy activity there.

Energy supplied by Arctic Atlantification

Given the marked increase in baroclinic energy conversion in the Eurasian Basin, it is crucial to understand the mechanisms that sustain this process. Changes in both vertical stratification and horizontal density gradients are known to influence baroclinic energy conversion processes[43,47]. In particular, the Mean Available Potential Energy (MAPE) associated with the large-scale density field can be transferred to EAPE through baroclinic instability and subsequently converted into EKE. To understand how large-scale oceanic changes drive the intensification of eddy activity in the deep Eurasian Basin, this section examines the temporal evolution of MAPE and its conversion to EAPE, as detailed in Eqs. (6) and (8) in "Methods."

With the progression of Arctic Atlantification, temperatures in the Eurasian Basin are projected to rise under future warming scenarios[16,48] (Fig. 4a, b and Supplementary Fig. 6a, b). A pronounced warming trend is evident throughout the upper 1000 m of the water column. This warming is attributed not only to increasing temperature of the inflowing Atlantic Water but also to the enhanced inflow through both the Fram Strait and the Barents Sea Opening (Supplementary Fig. 7). Concurrently, salinity in the deep layer is projected to decline slightly (Fig. 4c, d and Supplementary Fig. 6c, d). This freshening results from increased surface freshwater flux along the Atlantic Water current before reaching the Arctic Basin and a weakening of the Atlantic Meridional Overturning Circulation, which reduces poleward salt transport[16,49]. The subsurface density decreases accordingly, accompanied by steepening of the isopycnals and an intensification of the lateral density gradient, particularly along the continental slope (Fig. 4e, f and Supplementary Fig. 6e, f). We isolate the effects of warming and freshening by recomputing future density while substituting

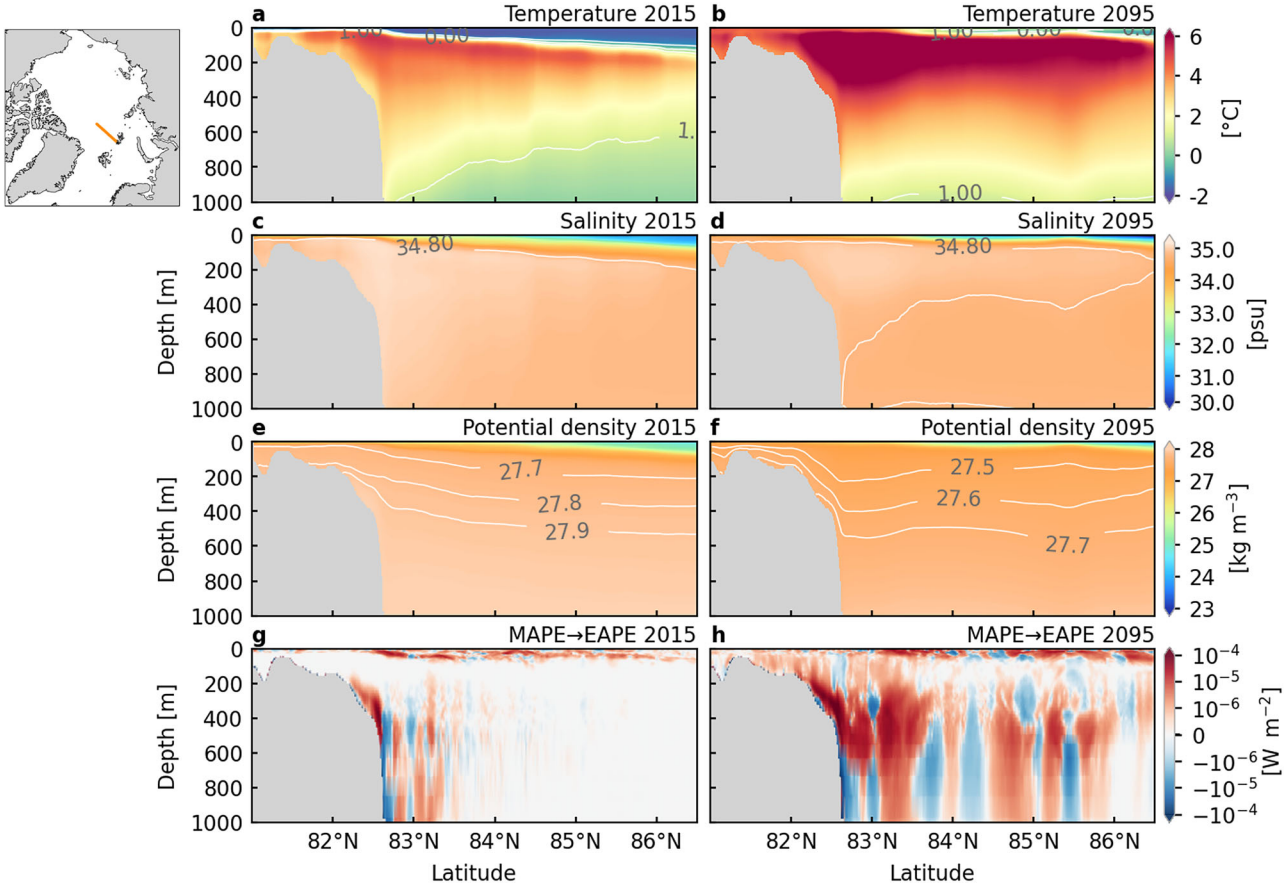

Fig. 4 | Arctic Atlantification supplies energy for eddy generation. Vertical transects of temperature in (**a**) 2015 and (**b**) 2095. **c**, **d** Same as (**a**, **b**), but for salinity. **e**, **f** Same as (**a**, **b**), but for potential density. **g**, **h** Same as (**a**, **b**), but for conversion rate from mean available potential energy (MAPE) to eddy available potential energy (EAPE) ($C_{\mathrm{MAPE}\rightarrow\mathrm{EAPE}}$). The solid yellow line in the top-left inset indicates the location of the transect in the western Eurasian Basin.

either temperature or salinity with present-day values. Both changes strengthen the lateral density gradient near the continental slope, with warming contributing more than freshening (Supplementary Fig. 8).

The MAPE is projected to increase by 74% in the deep Eurasian Basin under the future warming condition (Fig. 5f). The conversion rate from MAPE to EAPE ($C_{\mathrm{MAPE}\rightarrow\mathrm{EAPE}}$) is also projected to rise (Fig. 4g, h and Supplementary Fig. 6g, h). When integrated over the deep layer of the Eurasian Basin, this conversion rate increases by more than 5 times in the warming scenario considered (Fig. 5b). Even when the contribution of vertical stratification is excluded from the calculation (by multiplying vertical stratification to equation 8), the value still increases by nearly 5 times (Fig. 5d). This indicates the dominant role of the lateral density gradient and mesoscale eddy density flux in enhancing the energy conversion, although the weakened vertical stratification in the upper portion of the deep layer (Supplementary Fig. 5) contributes slightly. The excess EAPE under the warming scenario is subsequently converted into EKE (Supplementary Figs. 9 and 10), leading to a substantial intensification of eddy activities in the deep ocean layer.

In the upper layer, without changes in vertical stratification, the conversion rate from MAPE to EAPE would increase by about a factor of four under the warming scenario (Fig. 5c). However, vertical stratification in the upper layer is projected to strengthen markedly (Supplementary Fig. 5). Because the conversion rate depends oppositely on the lateral density gradient and vertical stratification (Eq. (8)), the enhanced stratification offsets part of the increase driven by the strengthened lateral density gradient, reducing the net increase to less than a factor of three (Fig. 5a). This imposes a constraint on the intensification of EKE in the surface layer, partially offsetting the effect of reduced surface friction. Thus, while stratification changes have only a minor influence on EKE in the deep layer, their impact in the upper layer is non-negligible.

Discussion

Using a global ocean-sea ice model with 1 km horizontal resolution in the Arctic, we demonstrate that continued Arctic Atlantification under future climate warming substantially energizes the deep Arctic Ocean, particularly the Eurasian Basin, primarily by intensifying eddy activity. The Eurasian Basin displays enhanced eddy activity throughout depth, standing in opposition to the global-mean trend of increased stratification and declining EKE in the deep ocean reported before[13]. Comparing our two sets of model simulations indicates that eddy-resolving resolution is required to fully capture the magnitude of the increase in eddy activity, although the overall tendency is also evident in eddy-permitting simulations.

An increase in deep-ocean EKE is discernible across the Arctic Ocean, with the strongest enhancement in the Eurasian and Makarov Basins, where Arctic Atlantification exerts the greatest influence. Atlantification increases the reservoir of mean available potential energy and promotes its conversion into EKE. The TKE in the Arctic Basin is projected to rise by 140% by the late 21st century, with approximately 80% of this increase attributable to intensified EKE, including 60% arising from EKE in the deep ocean layer experiencing strengthened Atlantification. It is important to note that these quantitative results are based on the SSP5-8.5 scenario and should therefore be viewed as an upper-bound estimate of potential future changes.

Ocean eddies have been suggested to play an important role in driving and modulating a range of key processes in the Arctic Ocean. An intensification of eddy activity has the potential to enhance the lateral transport of

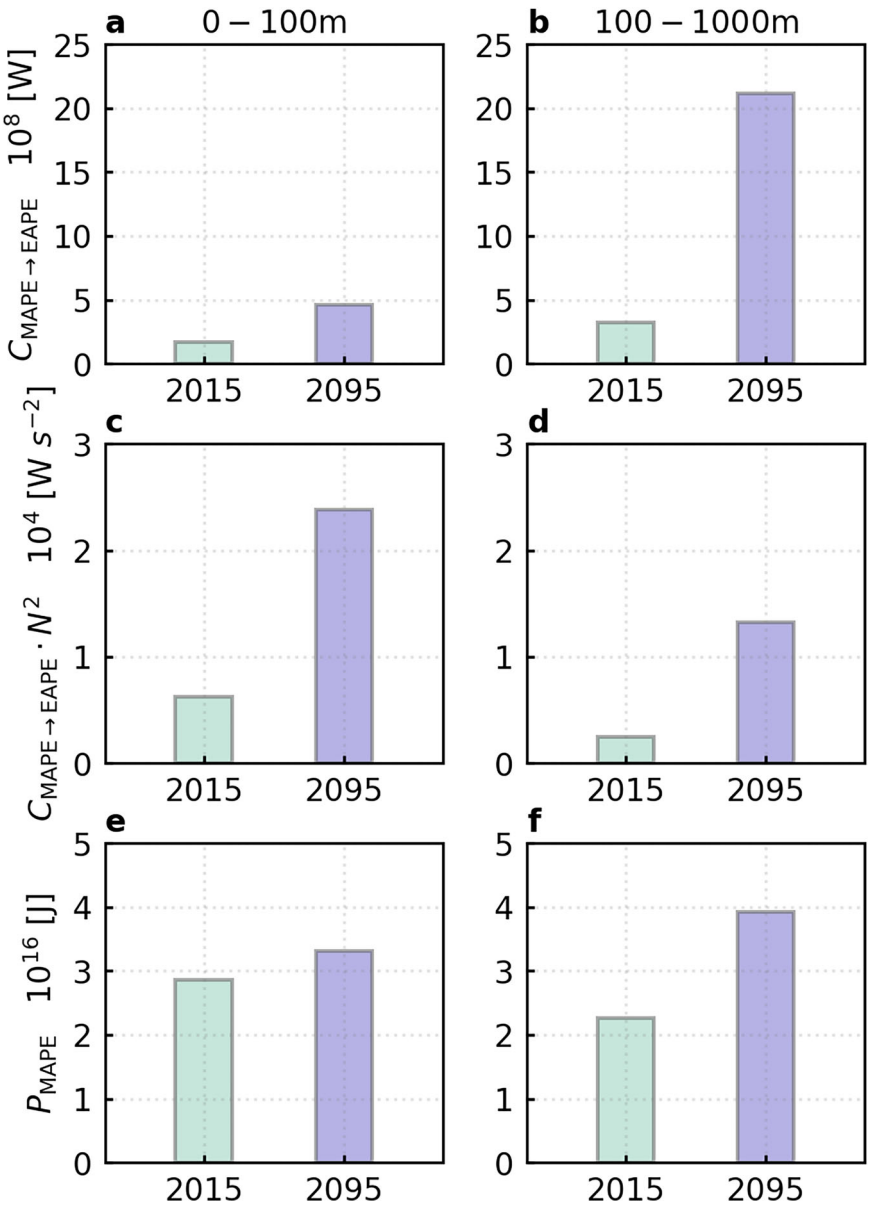

Fig. 5 | Influence of horizontal density gradients and vertical stratification on energy conversion. a, **b** Vertically and horizontally integrated conversion rates from mean available potential energy (MAPE) to eddy available potential energy (EAPE) ($C_{MAPE \rightarrow EAPE}$) for 2015 and 2095 in the Eurasian Basin: (**a**) upper layer of 0–100 m depth range and (**b**) deep layer of 100–1000 m depth range. **c**, **d** Same as (**a**, **b**), but for $C_{MAPE \rightarrow EAPE} \cdot N^2$. **e**, **f** Same as (**a**, **b**), but for MAPE (P_{MAPE}).

water masses and momentum from boundary currents into the basin interior[24,37], and to strengthen vertical heat flux[17,46]. Our simulations show a substantial increase in upward eddy heat flux in the Eurasian Basin in the future warming scenario (Supplementary Fig. 12). Arctic Atlantification is projected to intensify under climate warming, with strong Arctic Ocean warming driven by increasing transport of oceanic heat through the Fram Strait and Barents Sea Opening[16,50]. Surplus ocean heat can contribute to sea ice decline in much of the Arctic region[51,52]. Eddies could exacerbate sea ice basal melting by vertically transporting ocean heat and laterally advecting sea ice and warm water[17,53,54]. The simulated increase in vertical eddy heat flux (Supplementary Fig. 12) suggests that these eddy-driven processes are likely to intensify in the future. Further studies are needed to better quantify the role of enhanced eddy activity throughout the upper and deep layers in future Arctic sea ice decline.

Lateral transport and energy backscatter also act to weaken the density gradients that drive EKE growth and to enhance dissipation, thereby limiting eddy activity intensification[55–57]. Beyond their physical significance, eddies also shape biogeochemical processes by modulating primary productivity and vertical carbon export through multiple mechanisms[58,59]. For instance, they facilitate the transport of biomass from the extensive shelf region into the deep central basin[18]. Consequently, a sustained increase in EKE under future climate conditions not only substantially energizes the Eurasian and Makarov Basins, but may be also poised to strengthen the coupling between large-scale circulation changes and ecosystem responses. Therefore, Arctic Atlantification may exert a stronger influence on the Arctic climate and marine ecosystems than previously recognized, particularly through enhancing kinetic energy. Future dedicated studies are required to assess these implications.

Methods

Model simulations

The model data used in this study are derived from simulations conducted with the Finite-volume Sea ice Ocean Model version 2 (FESOM2), which solves the ocean primitive equations on unstructured triangular meshes[60]. FESOM2 employs a finite volume discretization on prismatic meshes, allowing for variable horizontal resolution without requiring nested grids. Its sea ice component, the Finite-Element Sea Ice Model (FESIM), operates on the same unstructured mesh as the ocean component[61]. The model performs well in simulating the global ocean, with improved computational efficiency than its previous version[62–64]. It can reasonably reproduce

observed Arctic Ocean changes when forced by reanalysis atmospheric forcing[65].

The simulations employed in this study have been described in detail in previous work[30]. A brief summary is provided here for completeness. Two model configurations were used. The high-resolution setup features a horizontal resolution of 1 km within the Arctic Ocean and 30 km outside this region. It includes 70 unevenly spaced vertical levels, with 5 m vertical spacing in the upper 100 m, gradually increasing with depth. This fine resolution allows for an adequate representation of the mesoscale eddy activity field in the Arctic Ocean, with the exception of continental shelf regions[26]. Due to its high computational cost, it remains challenging to run century-long simulations. The second configuration is a medium-resolution simulation with a horizontal resolution of 4.5-km in the Arctic Ocean. This setup is computationally more efficient, enabling longer simulations.

The 4.5-km resolution simulation spans the period from 1958 to 2100 and is initialized using the Polar Science Center Hydrographic Climatology dataset (PHC3.0)[66]. Atmospheric forcing and river runoff inputs are derived from the CMIP6 outputs of the coupled climate model AWI-CM1[67,68], covering the historical period from 1958 to 2014 and the future high-emission SSP5-8.5 scenario from 2015 to 2100[39]. We choose SSP5-8.5 because our aim is to elucidate the dynamical mechanisms driving future changes in the deep Arctic Ocean, and this high-emission scenario provides a relatively large signal-to-noise ratio (i.e., stronger forced trends compared with internal variability). An equivalent high-emission pathway has also been used in previous studies of global deep-ocean eddy activity[13], enabling more direct intercomparison.

Ocean and sea ice outputs from the 4.5-km resolution simulation at the ends of 2009 and 2089 were interpolated onto the 1-km resolution mesh. Using these interpolated fields as initial conditions, two 1-km resolution simulations were conducted using the same atmospheric forcing as in the 4.5-km resolution setup, each covering a 6-year period: 2010–2015 and 2090–2095. For each simulation slice, the first two years were considered as spin-up, while the remaining four years were used for analysis. These two high-resolution slice simulations represent present and future climates, respectively.

Ocean kinetic energy

The TKE and its two components are calculated as follows:

$$\mathrm{TKE} = \int_V \frac{1}{2}\rho_0\left(\overline{u^2}+\overline{v^2}\right) dV \tag{1}$$

$$\mathrm{MKE} = \int_V \frac{1}{2}\rho_0\left(\overline{u}^2+\overline{v}^2\right) dV \tag{2}$$

$$\mathrm{EKE} = \int_V \frac{1}{2}\rho_0\left(\overline{u'^2+v'^2}\right)dV = \int_V \left[\frac{1}{2}\rho_0\left(\overline{u^2}+\overline{v^2}\right) - \frac{1}{2}\rho_0\left(\overline{u}^2+\overline{v}^2\right)\right] dV, \tag{3}$$

where ρ_0 is the constant reference density, $\int_V dV$ indicates the volume integral over the ocean domain. u and v are the zonal and meridional velocities, $\overline{u}^2$ and $\overline{v}^2$ are the squares of the annual mean velocities. To illustrate the spatial distribution of kinetic energy, we also computed the vertically integrated values at each horizontal location.

Here, EKE is defined using Reynolds decomposition. Under this definition, EKE captures not only coherent eddies, but also the variability associated with meanders and jets. It is therefore often used as a metric of eddy activity, since meanders and jets are an inherent part of mesoscale variability[11–13,47]. We adopt this definition within the Lorenz Energy Cycle framework, which allows changes in EKE to be explained in terms of correspondingly defined energy transfer terms[47].

Energy conversion to EKE

To elucidate the main energy sources of enhanced deep Arctic Ocean EKE, we analyzed the energy conversion rates from eddy available potential energy (EAPE) to EKE and from MKE to EKE[42,47,69]:

$$C_{\mathrm{EAPE}\to\mathrm{EKE}} = -\int_V g\,\overline{\rho' w'}\, dV \tag{4}$$

$$C_{\mathrm{MKE}\to\mathrm{EKE}} = -\int_V \rho_0\left(\overline{u'\mathbf{u}'}\cdot\nabla\overline{u} + \overline{v'\mathbf{u}'}\cdot\nabla\overline{v}\right) dV, \tag{5}$$

where g is the gravitational acceleration, w' and ρ' represent the temporal deviations from the mean vertical velocity $\overline{w}$ and the mean density $\overline{\rho}$ respectively, defined as $w' = w - \overline{w}$ and $\rho' = \rho - \overline{\rho}$. The energy conversion rate from component A to component B is denoted by $C_{A\to B}$, and a negative value of $C_{A\to B}$ indicates an effective energy conversion from B to A. Accordingly, $C_{\mathrm{EAPE}\to\mathrm{EKE}}$ and $C_{\mathrm{MKE}\to\mathrm{EKE}}$ represent the baroclinic energy conversion rate from EAPE to EKE, and barotropic energy conversion rate from MKE to EKE, respectively.

Mean available potential energy and conversion

Mean available potential energy describes the potential energy available associated with the departure of the time-mean density from the stable state, defined as follows[47,70]:

$$P_{\mathrm{MAPE}} = -\int_V \frac{1}{2}\frac{g}{n_0}\overline{\rho^*}^2\, dV, \tag{6}$$

where the time-mean density anomaly ρ^* is

$$\rho^* = \rho - \rho_{ref}, \tag{7}$$

n_0 denotes the vertical gradient of the time-mean and area-mean background potential density. Following von Storch et al.[47], the reference density ρ_{ref} is defined as the area-averaged, time-mean density at each model level, so the density anomalies reflect horizontal deviations at each depth level, which are associated with baroclinic instability.

The conversion rate from MAPE to EAPE is given by:

$$C_{\mathrm{MAPE}\to\mathrm{EAPE}} = \int_V \frac{g}{n_0}\overline{\rho'\mathbf{u}'}\cdot\nabla_h\overline{\rho}\, dV, \tag{8}$$

where $\overline{\rho'\mathbf{u}'}$ is the eddy density flux and $\nabla_h\overline{\rho}$ is the horizontal density gradient. $C_{\mathrm{MAPE}\to\mathrm{EAPE}}$ describes the transfer of potential energy from the large-scale mean state to density perturbations. A positive value of $C_{\mathrm{MAPE}\to\mathrm{EAPE}}$ indicates that mesoscale eddies are gaining available potential energy by extracting it from the background stratification maintained by the mean flow. All variables are defined on the model grid, and time averaging is performed over the analysis period. The area-mean calculations of n_0 and ρ_{ref} are based on the Arctic domain. The model outputs required for the calculation of Eqs. (7) and (8) are available for 2015 and 2095.

Uncertainties and limitations

The reliability of our climate projection depends on the quality of the atmospheric forcing and the model's capacity to represent essential ocean dynamics. While the model configurations employed here enable high-resolution representation of Arctic Ocean mesoscale processes, the inherent uncertainties and limitations should be considered when interpreting the results.

The atmospheric forcing used in this study is derived from the CMIP6 simulations of the coupled model AWI-CM1. In the SSP585 scenario, AWI-CM1 projects a global-mean surface warming of approximately 4K in the 2090s above the 2000–2015 level, very similar to the multi-model-mean result of CMIP6 models[68]. Previous evaluation of the simulations used in this study shows that they successfully reproduce the satellite-observed decline trend in Arctic sea ice extent in the historical period, and the simulated timing of an emerging seasonally ice-free Arctic in September in the 2050s is consistent with the CMIP6 multi-model-mean

result[30]. The model has a reasonable representation of temperature, salinity, and stratification for the historical period, but model biases are clearly present (Supplementary Fig. 11), indicating potential uncertainty in future projections. As FESOM2 biases in simulated Arctic Ocean temperature and salinity were found to be smaller when it is driven by atmospheric reanalysis fields[65], the model biases in the current simulations should be mainly due to the atmospheric forcing biases stemming from the AWI-CM1 CMIP6 simulations.

The 4.5-km resolution simulation was performed continuously with a long spinup, while the 1-km resolution simulations were restarted from the corresponding years of the 4.5-km resolution simulation, reducing the required spin-up time. A two-year re-spinup is still relatively short, but represents a practical choice given computational constraints. In Fig. 2, EKE in the high-resolution simulations clearly stands out from the medium-resolution background, indicating that mesoscale dynamics spin up rapidly and reach a distinct energetic state within two years. Nevertheless, the short re-spinup may still lead to some underestimation of EKE in the 1-km high-resolution simulations. In addition, while eddy activity spins up rapidly, the large-scale properties of the Atlantic Water layer at depth likely require longer timescales to equilibrate. The evolution of the Atlantic Water layer is influenced by the cumulative effects of eddies, such as vertical eddy heat flux (Supplementary Fig. 12). Therefore, long-term 1-km resolution simulations are required to fully assess the feedbacks between large-scale and mesoscale processes in their equilibrium states. Furthermore, the ocean-sea ice model was driven by prescribed atmospheric forcing without coupling to an active atmospheric model. Although this strategy allows us to perform projections with very high resolutions, it might lead to a conservative estimate of EKE in the upper layer because kinetic energy transferred from ocean to atmosphere does not give feedback in this case[71]. Moreover, the slice simulation in the future period (2092–2095) may, by chance, correspond to a relatively energetic phase associated with internal variability, potentially leading to a slight overestimation of the projected changes, as this period is used to represent end-of-century conditions. However, the overall conclusions remain robust, as the time-depth plots of kinetic energy show a clear upward trend (Fig. 2).

Long-term mean velocity is commonly used to compute MKE in practice[11,13,47]. Here, to minimize the contribution of interannual and decadal variability to EKE, we use annual-mean velocity for the Reynolds decomposition. However, the resulting MKE still contains some eddy contributions (Fig. 1e). This implies that we should not shorten the averaging period further. A slightly modified Reynolds decomposition was applied to remove seasonal variability from EKE[72]. Their method, however, does not strictly enforce the identity TEK=MKE+EKE. While the associated residual is reported to be small for their specific application, it is not guaranteed to remain small in other settings and would need to be evaluated case by case. This is particularly relevant for Lorenz Energy Cycle diagnostics: the energy conversion terms should be consistent with the adopted MKE and EKE definition. If the decomposition is not energy-conserving, analogous residuals may also affect conversion rates, and the magnitude of these impacts is unknown. Any definition involves trade-offs. We therefore adopt annual means, consistent with previous Arctic Ocean studies[69]. The EKE definition here represents kinetic energy associated with all temporal variability relative to the mean flow and does not uniquely isolate coherent mesoscale eddies. Variability on timescales shorter than one year is included in EKE and may therefore lead to a quantitative overestimate. However, as noted above, using a shorter averaging window would instead underestimate EKE. Our choice thus represents a pragmatic compromise between averaging periods that are too long and too short. Importantly, our central result is robust: energy conversions toward EKE across the stages of the Lorenz Energy Cycle are projected to increase substantially in the future, providing a theoretical basis for the simulated increase in eddy activity under climate warming. Therefore, our main conclusion is not sensitive to the specific EKE definition.

We compute kinetic energy and energy conversion rates for two layers with fixed depths. With the layer thickness held constant, changes in layer-integrated EKE directly reflect changes in eddy activity because the analyzed ocean volume is unchanged. We find that EKE increases in the deep layer, most strongly in the Eurasian Basin. Our goal is to explain this identified change. The deep layer in the Eurasian Basin is occupied mainly by Atlantic Water in both considered scenarios, which simplifies the interpretation. In the future climate, the Atlantic Water layer is projected to become thicker than the fixed deep layer (100–1000 m); consequently, volume-integrated EKE increase for the full Atlantic Water layer would be larger than those estimated for the fixed layer. This does not, however, alter our interpretation of the mechanisms driving the dynamical changes in the deep Arctic Ocean. Because the Atlantic Water layer lies deeper in the western Arctic, the deep-layer changes there should not be attributed only to Atlantification. However, the deep-layer energization is weaker in the western Arctic than in the Eurasian Basin, the starting location of Arctic Atlantification, which supports our main conclusion that Atlantification plays an important role in the projected deep-ocean changes.

Data availability

The model data used to produce the paper figures are available at https://doi.org/10.5281/zenodo.15685929[73].

Received: 19 August 2025; Accepted: 2 April 2026;
Published online: 14 April 2026

References

1. Chelton, D. B., Schlax, M. G. & Samelson, R. M. Global observations of nonlinear mesoscale eddies. *Prog. Oceanogr.* **91**, 167–216 (2011).
2. Ferrari, R. & Wunsch, C. Ocean circulation kinetic energy: reservoirs, sources, and sinks. *Annu. Rev. Fluid Mech.* **41**, 253–282 (2009).
3. Storer, B. A., Buzzicotti, M., Khatri, H., Griffies, S. M. & Aluie, H. Global energy spectrum of the general oceanic circulation. *Nat. Commun.* **13**, 5314 (2022).
4. Hallberg, R. & Gnanadesikan, A. The role of eddies in determining the structure and response of the wind-driven Southern Hemisphere overturning: results from the modeling eddies in the Southern Ocean (MESO) project. *J. Phys. Oceanogr.* **36**, 2232–2252 (2006).
5. Dong, C., McWilliams, J. C., Liu, Y. & Chen, D. Global heat and salt transports by eddy movement. *Nat. Commun.* **5**, 3294 (2014).
6. Zhang, Z., Wang, W. & Qiu, B. Oceanic mass transport by mesoscale eddies. *Science* **345**, 322–324 (2014).
7. Zhao, J. et al. Maintenance of mid-latitude oceanic fronts by mesoscale eddies. *Sci. Adv.* **6**, eaba7880 (2020).
8. Falkowski, P. G., Ziemann, D., Kolber, Z. & Bienfang, P. K. Role of eddy pumping in enhancing primary production in the ocean. *Nature* **352**, 55–58 (1991).
9. Keppler, L. et al. Effects of mesoscale eddies on Southern Ocean biogeochemistry. *AGU Adv.* **5**, e2024AV001355 (2024).
10. Griffies, S. M. et al. Impacts on ocean heat from transient mesoscale eddies in a hierarchy of climate models. *J. Clim.* **28**, 952–977 (2015).
11. Martínez-Moreno, J. et al. Global changes in oceanic mesoscale currents over the satellite altimetry record. *Nat. Clim. Change* **11**, 397–403 (2021).
12. Beech, N. et al. Long-term evolution of ocean eddy activity in a warming world. *Nat. Clim. Change* **12**, 910–917 (2022).
13. Wang, S. et al. A more quiescent deep ocean under global warming. *Nat. Clim. Change* **14**, 961–967 (2024).
14. Peng, Q. et al. Surface warming-induced global acceleration of upper ocean currents. *Sci. Adv.* **8**, eabj8394 (2022).
15. Rantanen, M. et al. The Arctic has warmed nearly four times faster than the globe since 1979. *Commun. Earth Environ.* **3**, 168 (2022).
16. Shu, Q. et al. Arctic Ocean Amplification in a warming climate in CMIP6 models. *Sci. Adv.* **8**, eabn9755 (2022).
17. Manucharyan, G. E. & Thompson, A. F. Heavy footprints of upper-ocean eddies on weakened Arctic sea ice in marginal ice zones. *Nat. Commun.* **13**, 2147 (2022).

18. Watanabe, E. et al. Enhanced role of eddies in the Arctic marine biological pump. *Nat. Commun.* **5**, 3950 (2014).
19. Timmermans, M.-L., Toole, J., Proshutinsky, A., Krishfield, R. & Plueddemann, A. Eddies in the Canada Basin, Arctic Ocean, observed from Ice-Tethered Profilers. *J. Phys. Oceanogr.* **38**, 133–145 (2008).
20. Dmitrenko, I. A., Kirillov, S. A., Ivanov, V. V. & Woodgate, R. A. Mesoscale Atlantic water eddy off the Laptev Sea continental slope carries the signature of upstream interaction. *J. Geophys. Res. Oceans* **113** C07005 (2008).
21. Zhao, M. et al. Characterizing the eddy field in the Arctic Ocean halocline. *J. Geophys. Res. Oceans* **119**, 8800–8817 (2014).
22. Muench, R. D., Gunn, J. T., Whitledge, T. E., Schlosser, P. & Smethie Jr, W. An Arctic Ocean cold core eddy. *J. Geophys. Res. Oceans* **105**, 23997–24006 (2000).
23. Kozlov, I. E., Artamonova, A. V., Manucharyan, G. E. & Kubryakov, A. A. Eddies in the western Arctic Ocean from spaceborne SAR observations over open ocean and marginal ice zones. *J. Geophys. Res. Oceans* **124**, 6601–6616 (2019).
24. Spall, M. A., Pickart, R. S., Fratantoni, P. S. & Plueddemann, A. J. Western Arctic shelfbreak eddies: formation and transport. *J. Phys. Oceanogr.* **38**, 1644–1668 (2008).
25. Armitage, T. W. K., Manucharyan, G. E., Petty, A. A., Kwok, R. & Thompson, A. F. Enhanced eddy activity in the Beaufort Gyre in response to sea ice loss. *Nat. Commun.* **11**, 761 (2020).
26. Wang, Q. et al. Eddy kinetic energy in the Arctic Ocean from a global simulation with a 1-km Arctic. *Geophys. Res. Lett.* **47**, e2020GL088550 (2020).
27. von Appen, W.-J. et al. Eddies and the distribution of eddy kinetic energy in the Arctic Ocean. *Oceanography* **35**, 42–51 (2022).
28. Zhao, M. & Timmermans, M.-L. Vertical scales and dynamics of eddies in the Arctic Ocean's Canada Basin. *J. Geophys. Res. Oceans* **120**, 8195–8209 (2015).
29. Meneghello, G. et al. Genesis and decay of mesoscale baroclinic eddies in the seasonally ice-covered interior Arctic Ocean. *J. Phys. Oceanogr.* **51**, 115–129 (2021).
30. Li, X. et al. Eddy activity in the Arctic Ocean projected to surge in a warming world. *Nat. Clim. Change* **14**, 156–162 (2024).
31. Polyakov, I. V. et al. Greater role for Atlantic inflows on sea-ice loss in the Eurasian Basin of the Arctic Ocean. *Science* **356**, 285–291 (2017).
32. Ingvaldsen, R. B. et al. Physical manifestations and ecological implications of Arctic Atlantification. *Nat. Rev. Earth Environ.* **2**, 874–889 (2021).
33. Wang, Q., Shu, Q. & Wang, F. Recent emergence of Arctic Atlantification dominated by climate warming. *Sci. Adv.* **10**, eadq5235 (2024).
34. Polyakov, I. V. et al. Atlantification advances into the Amerasian Basin of the Arctic Ocean. *Sci. Adv.* **11**, eadq7580 (2025).
35. Årthun, M., Eldevik, T. & Smedsrud, L. H. The role of Atlantic heat transport in future Arctic winter sea ice loss. *J. Clim.* **32**, 3327–3341 (2019).
36. Nurser, G. & Bacon, S. The Rossby radius in the Arctic Ocean. *Ocean Sci.* **10**, 967–975 (2014).
37. Timmermans, M.-L. & Marshall, J. Understanding Arctic Ocean circulation: a review of ocean dynamics in a changing climate. *J. Geophys. Res. Oceans* **125**, e2018JC014378 (2020).
38. Liu, C. et al. Spatial scales of kinetic energy in the Arctic Ocean. *J. Geophys. Res. Oceans* **129**, e2023JC020013 (2024).
39. O'Neill, B. et al. The scenario model intercomparison project (ScenarioMIP) for CMIP6. *Geosci. Model Dev.* **9**, 3461–3482 (2016).
40. Rudels, B. & Carmack, E. Arctic Ocean water mass structure and circulation. *Oceanography* **35**, 82–91 (2022).
41. Polyakov, I. V. et al. Weakening of cold halocline layer exposes sea ice to oceanic heat in the eastern Arctic Ocean. *J. Clim.* **33**, 8107–8123 (2020).
42. Beckmann, A., Böning, C. W., Brügge, B. & Stammer, D. On the generation and role of eddy variability in the central North Atlantic Ocean. *J. Geophys. Res. Oceans* **99**, 20381–20391 (1994).
43. Tulloch, R., Marshall, J., Hill, C. & Smith, K. S. Scales, growth rates, and spectral fluxes of baroclinic instability in the ocean. *J. Phys. Oceanogr.* **41**, 1057–1076 (2011).
44. Scott, R. B. & Wang, F. Direct evidence of an oceanic inverse kinetic energy cascade from satellite altimetry. *J. Phys. Oceanogr.* **35**, 1650–1666 (2005).
45. Waterman, S. Eddy–mean flow interactions in western boundary current jets. *J. Phys. Oceanogr.* **40**, 1014–1031 (2010).
46. Müller, V. et al. Variability of eddy kinetic energy in the Eurasian Basin of the Arctic Ocean inferred from a model simulation at 1-km resolution. *J. Geophys. Res. Oceans* **129**, e2023JC020139 (2024).
47. von Storch, J.-S. et al. An estimate of the Lorenz Energy Cycle for the world ocean based on the STORM/NCEP simulation. *J. Phys. Oceanogr.* **42**, 2185–2205 (2012).
48. Khosravi, N. et al. The Arctic Ocean in CMIP6 models: biases and projected changes in temperature and salinity. *Earths Future* **10**, e2021EF002282 (2022).
49. Wang, S., Wang, Q., Wang, M., Lohmann, G. & Qiao, F. Arctic Ocean freshwater in CMIP6 coupled models. *Earths Future* **10**, e2022EF002878 (2022).
50. Wang, Q. et al. A review of Arctic–Subarctic Ocean linkages: past changes, mechanisms, and future projections. *Ocean Land Atmos. Res.* **2**, 0013 (2023).
51. Dörr, J., Årthun, M., Eldevik, T. & Sandø, A. B. Expanding influence of Atlantic and Pacific Ocean heat transport on winter sea-ice variability in a warming Arctic. *J. Geophys. Res. Oceans* **129**, e2023JC019900 (2024).
52. Cheng, K. et al. Distinct impacts of increased Atlantic and Pacific Ocean heat transport on Arctic Ocean warming and sea ice decline. *J. Geophys. Res. Oceans* **130**, e2024JC021178 (2025).
53. Gupta, M., Marshall, J., Song, H., Campin, J.-M. & Meneghello, G. Sea-ice melt driven by ice-ocean stresses on the mesoscale. *J. Geophys. Res. Oceans* **125**, e2020JC016404 (2020).
54. Martínez-Moreno, J., Lique, C. & Talandier, C. Sea ice heterogeneity as a result of ocean eddy activity during the ice growth season. *Geophys. Res. Lett.* **52**, e2024GL113645 (2025).
55. Kang, D. & Curchitser, E. N. Energetics of eddy–mean flow interactions in the Gulf Stream Region. *J. Phys. Oceanogr.* **45**, 1103–1120 (2015).
56. Yan, X., Kang, D., Curchitser, E. N. & Pang, C. Energetics of eddy–mean flow interactions along the western boundary currents in the north pacific. *J. Phys. Oceanogr.* **49**, 789–810 (2019).
57. Li, J., Roughan, M. & Kerry, C. Dynamics of interannual eddy kinetic energy modulations in a western boundary current. *Geophys. Res. Lett.* **48**, e2021GL094115 (2021).
58. Schourup-Kristensen, V., Wekerle, C., Wolf-Gladrow, D. A. & Völker, C. Arctic ocean biogeochemistry in the high resolution FESOM 1.4-REcoM2 model. *Prog. Oceanogr.* **168**, 65–81 (2018).
59. MacKinnon, J. A. et al. A warm jet in a cold ocean. *Nat. Commun.* **12**, 2418 (2021).
60. Danilov, S., Sidorenko, D., Wang, Q. & Jung, T. The Finite-volume sea ice–ocean model (FESOM2). *Geosci. Model Dev.* **10**, 765–789 (2017).
61. Danilov, S. et al. Finite-element sea ice model (FESIM), version 2. *Geosci. Model Dev.* **8**, 1747–1761 (2015).
62. Scholz, P. et al. Assessment of the Finite-volume Sea ice–Ocean Model (FESOM2.0) – Part 1: description of selected key model elements and comparison to its predecessor version. *Geosci. Model Dev.* **12**, 4875–4899 (2019).
63. Scholz, P. et al. Assessment of the Finite-volume Sea ice–Ocean Model (FESOM2.0) – Part 2: partial bottom cells, embedded sea ice and vertical mixing library CVMix. *Geosci. Model Dev.* **15**, 335–363 (2022).

64. Koldunov, N. V. et al. Scalability and some optimization of the Finite-volume Sea ice–Ocean Model, version 2.0 (FESOM2). *Geosci. Model Dev.* **12**, 3991–4012 (2019).
65. Wang, Q. et al. Impact of increased resolution on Arctic Ocean simulations in Ocean Model Intercomparison Project phase 2 (OMIP-2). *Geosci. Model Dev.* **17**, 347–379 (2024).
66. Steele, M., Morley, R. & Ermold, W. PHC: a global ocean hydrography with a high-quality Arctic Ocean. *J. Clim.* **14**, 2079–2087 (2001).
67. Sidorenko, D. et al. Towards multi-resolution global climate modeling with ECHAM6-FESOM. Part I: model formulation and mean climate. *Clim. Dyn.* **44**, 757–780 (2015).
68. Semmler, T. et al. Simulations for CMIP6 with the AWI Climate Model AWI-CM-1-1. *J. Adv. Model. Earth Syst.* **12**, e2019MS002009 (2020).
69. Regan, H., Lique, C., Talandier, C. & Meneghello, G. Response of total and eddy kinetic energy to the recent spinup of the Beaufort Gyre. *J. Phys. Oceanogr.* **50**, 575–594 (2020).
70. Lorenz, E. N. Available potential energy and the maintenance of the general circulation. *Tellus* **7**, 157–167 (1955).
71. Renault, L., Molemaker, M., Gula, J., Masson, S. & McWilliams, J. C. Control and stabilization of the Gulf Stream by oceanic current interaction with the atmosphere. *J. Phys. Oceanogr.* **46**, 3439–3453 (2016).
72. Rieck, J. K., Martínez Moreno, J., Lique, C., Dufour, C. O. & Talandier, C. Mean kinetic energy and its projected changes dominate over eddy kinetic energy in the arctic ocean. *Geophys. Res. Lett.* **52**, e2025GL117957 (2025).
73. Chen, J. et al. *Energized Deep Ocean Induced by Arctic Atlanticification under Global Warming.Dataset, Zenodo* (2026).

Acknowledgements

The authors gratefully acknowledge Jan Streffing, Nikolay Koldunov, and Aleksei Koldunov for their assistance in understanding data structure and analysis scripts, and the Jülich Supercomputing Centre for providing computing time on the Earth System Modeling partition of the supercomputer JUWELS. X.D.W. discloses support for the research of this work from the National Natural Science Foundation of China (42225602). J.C. discloses support for the research of this work from the Postgraduate Research and Practice Innovation Program of Jiangsu Province (KYCX24_0808) and the scholarship program of China Scholarship Council (202306710106). X.Z.W. discloses support for the research of this work from Shanghai Frontiers Science Center of Polar Science (SCOPS, SOO2026-06) and CNOOC Marine Environmental and Ecological Protection Public Welfare Foundation (CF-MEEC/TR/2025-2). Q.W. discloses support for the research of this work from the German Helmholtz Climate Initiative REKLIM and the AWI INSPIRES program. X.L., V.M., S.D., and T.J. declare no relevant funding.

Author contributions

Q.W. and X.Z.W. conceived the study. J.C. analyzed the data and prepared the first draft of the manuscript under Q.W.'s supervision. XZ.W. supported the data analysis. X.L. performed the model simulations. V.M., S.D., XD.W., and T.J. contributed to scientific discussions. All authors contributed to paper revision.

Funding

Open Access funding enabled and organized by Projekt DEAL.

Competing interests

The authors declare no competing interests.

Additional information

Supplementary information The online version contains supplementary material available at https://doi.org/10.1038/s43247-026-03507-x.

Correspondence and requests for materials should be addressed to Qiang Wang.

Peer review information *Communications Earth and Environment* thanks Yueng-Djern Lenn and the other anonymous reviewer(s) for their contribution to the peer review of this work. Primary Handling Editors: Jennifer Veitch and Alice Drinkwater. A peer review file is available.